# Quasifree electron bremsstrahlung induced by 20-MeV-proton impact


doi: 10.1103/PhysRevA.24.1720

PHYSICAL REVIEW A VOLUME 24, NUMBER 4 OCTOBER 1981

# Quasifree electron bremsstrahlung induced by 20-MeV-proton impact

T. C. Chu
*Health Physics Division, National Tsing Hua University, Hsinchu, Taiwan 300, China*

K. Ishii and A. Yamadera
*Cyclotron and Radioisotope Center, Tohoku University, Sendai, 980 Japan*

M. Sebata and S. Morita
*Department of Physics, Faculty of Science, Tohoku University, Sendai, 980 Japan*

(Received 27 February 1981)

Energy spectra and angular distributions of quasifree electron bremsstrahlung (QFEB) induced by 20-MeV-proton bombardments of a Be target have been measured with a Si (Li) detector. The Doppler shift of QFEB is clearly observed in the energy spectra and depends on the observation angle. The production cross section calculated from a free-electron approximation is compared with the experimental result and the agreement is quite satisfactory. The spectral shape near the high-energy end point of the QFEB definitely reflects the velocity distribution of the orbital electrons of the target atom. Angular distributions of secondary-electron bremsstrahlung were also measured and are compared with a calculation which includes relativistic retardation effects.

## I. INTRODUCTION

Continuum x rays produced by the bombardment of gaseous or solid targets with heavy charged particles or heavy ions have been interpreted in terms of molecular-orbital (MO) x rays, radiative electron capture (REC), radiative ionization (RI), and secondary-electron bremsstrahlung (SEB).[1-9] Direct processes such as MO and REC play an important role in heavy-ion impact, while multistep processes such as RI and SEB play a predominant role in light-ion impact. Recently,[10] we have observed a new continuum x-ray component coming from a kind of RI process in bombardments of Be, C, and Al targets with 6–40-MeV protons. The high-energy end of this component changes with the proton energy and has a $\frac{1}{2}m_e V_p^2$ dependence, where $m_e$ is the electron mass and $V_p$ is the projectile velocity. This energy dependence of the continuum x rays has been well explained in terms of bremsstrahlung produced by orbital electrons scattered in the projectile-Coulomb field. We have obtained satisfactory agreement of the experimental results with the bremsstrahlung calculated in the projectile frame assuming that the orbital electrons are free and at rest, i.e., the quasifree electron bremsstrahlung (QFEB). Since the QFEB is a process occurring in the projectile frame, the Doppler effect is expected to appear in the spectrum. This effect has been observed earlier in the projectile-energy dependence of the spectrum. In this paper, angular distributions of the QFEB from a Be target bombarded with 20-MeV protons are measured and the results are compared with theoretical calculations that take into account the correction for the Coulomb deflection. The effect of velocity distribution of the orbital electron on the spectral shape near the high-energy end of QFEB is calculated and is compared with the experimental results. Angular distributions of SEB are also obtained and are compared with calculations taking account of the relativisitic-retardation effect and the Coulomb-deflection effect.

## II. EXPERIMENTAL

Beams of 20-MeV protons from the Tohoku-University cyclotron bombarded a self-supporting Be target of 46-mg/cm$^2$ thickness, which was set in a scattering chamber newly built for measuring angular distributions and installed in the beam line described in Ref. 11. This chamber of 40-cm inner diameter has a sliding membrane with a window for the x-ray detector and is designed so that the angle between the target surface and the direction of x-ray detection is always kept constant. Hence, the self-absorption (absorptions of x rays in the air path and windows) is the same at all detection angles and the error due to absorption corrections cancels out. The overall experimental arrangement has been described in Ref. 11, where special care was taken to reduce background radiation, and it was ascertained that the background measured without a target was quite negligible so that only the radiation coming from the target was measured. Moreover, as can be seen in the previous paper,[10] the background due to $\gamma$ rays from nuclear reactions occurring in the target material was considerable for the Al and C targets, while the x-ray spectra for the Be target were quite consistent with the theoretical calculations without taking account of the contribution

 

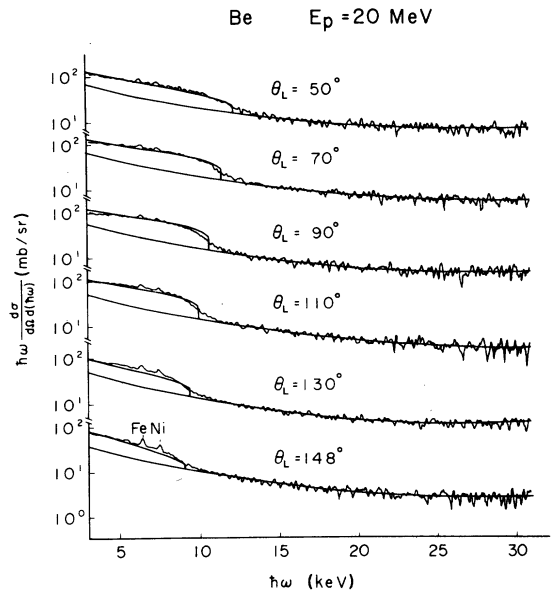


FIG. 1. Continuum x-ray spectra for the Be target bombarded with 20-MeV protons obtained over the angular range $\theta_L = 50$–$148°$. The ordinate shows the cross section multiplied by the x-ray energy. The smooth curves in the region 3–30 keV are obtained from the least-squares fit of Eq. (12) to the experimental results. The other curves show the sum of cross sections for SEB and for QFEB calculated from Eq. (5).

from $\gamma$ rays. This fact shows that the background due to $\gamma$ rays is negligible for the Be target.

Continuum x rays from the Be target (same as those used in the previous experiment) have been measured with an ORTEC Si (Li) detector at the angles $\theta_L = 50°$, 70°, 90°, 100°, 110°, 120°, 130°, 140°, and 148°. In order to avoid pileup effect, counting rates have been kept at about 100 cps. Production cross sections for continuum x rays, measured at angles $\theta_L = 50$–$148°$ and corrected for the detection efficiency and absorptions, are shown in Fig. 1, where the ordinate represents the production cross section multiplied by the x-ray energy—$[d\sigma^{br}/d\Omega\, d(\hbar\omega)]\hbar\omega$; this is a scaling based on the x-ray energy dependence of bremsstrahlung—$d\sigma^{br}/d\Omega\, d(\hbar\omega) = (1/\hbar\omega) f(\hbar\omega)$. Experimental errors have been estimated to be 15% at about 6 keV and 20% at about 15 keV from the following uncertainties: target thickness, 10%; detector efficiency and absorption corrections, 11%; and counting statistics, 0.2% and 14% at 6 keV and 15 keV, respectively.

## III. THEORETICAL

### A. QFEB

Theoretical treatments of the radiative-ionization process were first developed by Jakubassa and Kleber.[4] On the basis of the plane-wave Born approximation (PWBA), they calculated the radiative-ionization cross section for a case where the projectile velocity $V_p$ is larger than the velocity of the orbital electron $V_e$. For a case of $V_p < V_e$, Anholt and Saylor[9] have made calculations on the basis of the binary-encounter approximation (BEA). In the present case where $V_p$ is much larger than $V_e$, the orbital electron can be regarded as free and at rest, and radiative ionization is considered to be a bremsstrahlung produced by a free electron in the projectile frame, namely, QFEB. Under these conditions, the retardation effect and the Doppler effect can easily be introduced into the QFEB. In a previous paper,[10] QFEB was calculated in terms of a nonrelativisitc approximation. Here, the formula for QFEB is derived on the basis of the relativistic theory.

The production cross section for electron bremsstrahlung, including the first-order relativistic effect, is generally given in the center-of-mass system by[12]

$$\frac{d^2\sigma^{\mathrm{QFEB}}}{d\Omega\, d(\hbar\omega)}(T_r, \hbar\omega, \theta) = \begin{cases} 0 & \text{for } \hbar\omega > T_r, \\ \dfrac{Z_p^2}{\pi} Z_T \gamma_0^2 \alpha \dfrac{m_e C^2}{T_r \hbar\omega} g(\xi_0, \xi) \Big[ [\sin^2\theta + \tfrac{1}{4}(1+T)(3\cos^2\theta - 1)] \ln\Big(\dfrac{1+\sqrt{T}}{1-\sqrt{T}}\Big) - \tfrac{1}{2}\sqrt{T}(3\cos^2\theta - 1) \\ \quad + \dfrac{\beta}{2}\cos\theta[(7-T)\sin^2\theta + \tfrac{1}{2}(\cos^2\theta - \tfrac{3}{2}\sin^2\theta)(10T + 3 - 3T^2)] \\ \quad \times \ln\Big(\dfrac{1+\sqrt{T}}{1-\sqrt{T}}\Big) - 2\beta\sqrt{T}\cos\theta(\cos^2\theta - 2\sin^2\theta) \Big] & \text{for } \hbar\omega \le T_r. \end{cases} \quad (1)$$

Here, $Z_p$ and $Z_T$ are the atomic numbers of the projectile and the target nucleus, respectively, $\alpha$ is the fine-structure constant, $m_e C^2$ is the rest energy of electron, $\hbar\omega$ is the x-ray energy, $\theta$ is the emission angle of x rays with respect to the incident electron, and $T_r$ is the kinetic energy of the orbital electron relative to the projectile. Considering that the projectile mass is large in comparision with the electron mass, we approximately obtain

$$T_r = \tfrac{1}{2} m_e V_p^2 , \tag{2}$$

and $T$ and $\beta$ are defined by

$$\beta = \left(\frac{2T_r}{m_e C^2}\right)^{1/2}, \quad T = \frac{T_r - \hbar\omega}{T_r} . \tag{3}$$

Further, $g(\xi, \xi_0)$ is the correction term for the Coulomb deflection and is given by Sommerfeld[12] by

$$g(\xi_0, \xi) = \frac{\xi}{\xi_0} \frac{1 - e^{-2\pi\xi_0}}{1 - e^{-2\pi\xi}} ,$$

with

$$\xi_0 = Z_p \left(\frac{\mathcal{R}}{T_r}\right)^{1/2}, \quad \xi = Z_p \left(\frac{\mathcal{R}}{T_r \hbar\omega}\right)^{1/2} , \tag{4}$$

where $\mathcal{R}$ is the Rydberg constant.

The cross section $d^2\sigma^{\mathrm{QFEB}}/d\Omega\, d(\hbar\omega)$ has a finite value at the high-energy end $\hbar\omega = T_r$ because of the correction factor $g(\xi, \xi_0)$; whereas the PWBA calculation of $g(\xi_0, \xi) = 1$ gives $d^2\sigma^{\mathrm{QFEB}}/d\Omega\, d(\hbar\omega) = 0$ at $\hbar\omega = T_r$. It will be shown below that this difference between the two calculations plays an important role in the behavior of QFEB spectrum near the end-point energy.

Equation (1) represents the QFEB formula in the center-of-mass system of the projectile and the orbital electron. In order to compare with the experiment, this equation must be changed to that of the laboratory system by a Lorentz transformation[13] expressed by

$$\frac{d^2\sigma^{\mathrm{QFEB}}}{d\Omega_L\, d(\hbar\omega_L)}(T_r, \hbar\omega_L, \theta_L) = \frac{1 - \beta^2}{1 - \beta\cos\theta_L} \frac{d\sigma^{\mathrm{QFEB}}}{d\Omega\, d(\hbar\omega)}(T_r, \hbar\omega, \theta) ,$$
$$\hbar\omega = \frac{1 - \beta\cos\theta_L}{(1 - \beta^2)^{1/2}} \hbar\omega_L , \tag{5}$$

and

$$\cos\theta = -\frac{\cos\theta_L - \beta}{1 - \beta\cos\theta_L} .$$

Equation (5) has been obtained by assuming that the orbital electron is free and at rest.

Now, we will derive the QFEB formula for a free electron having the velocity components $(V_x, V_y, V_z)$. The relative kinetic energy $T_r'$ of the electron with respect to the projectile is

$$T_r' = T_r \left[\left(\frac{V_x}{V_p}\right)^2 + \left(\frac{V_y}{V_p}\right)^2 + \left(1 - \frac{V_z}{V_p}\right)^2\right], \tag{6}$$

where the $Z$ axis is taken in the direction of the incident beam. In the case of $V_p \gg V_e$, only the $Z$ component of the velocity contributes to $T_r'$, and Eq. (6) can be approximated by

$$T_r' \approx T_r \left(1 - \frac{V_z}{V_p}\right)^2 . \tag{7}$$

The velocity distribution function of orbital electrons in the $Z$ direction can be obtained by

$$\rho(V_z) = \int\int \rho(V_x, V_y, V_z) dV_x dV_y . \tag{8}$$

Here, $\rho(V_x, V_y, V_z)$ is the velocity distribution function of the orbital electrons; for example, it is given for the $1s$ electrons by[14]

$$\rho_{1s}(V_z) = \frac{8}{3\pi} \frac{V_0^5}{(V_0^2 + V_z^2)^3} ,$$

where $\frac{1}{2} m_e V_0^2$ is the binding energy for the $1s$ state. From the discussion described above and from Eqs. (5), (7), and (8), the QFEB formula taking account of the velocity distributions of Be $1s$ and $2s$ orbital electrons is expressed by

$$\sigma^{\mathrm{QFEB}}(\hbar\omega_L, \theta_L) = \int_{-\infty}^{V_p[1-(\hbar\omega/T_r)^{1/2}]} \frac{d^2\sigma^{\mathrm{QFEB}}}{d\Omega_L\, d(\hbar\omega_L)} \times (T_r', \hbar\omega_L, \theta_L)\rho(V_z) dV_z . \tag{9}$$

Here, the upper limit of the integration with respect to $V_z$ is determined from the condition $T_r' \geq \hbar\omega$.

### B. SEB

Theoretical calculations of SEB have been carried out by Folkmann *et al.*[5,6] by Jakubassa and Kleber,[3] and by Ishii *et al.*[7,8,10] We have also calculated the exact formula based on BEA. In a case of $V_p \gg V_e$ such as in the present one, however, we can assume that the orbital electrons are free and at rest as in the case of QFEB. Owing to this approximation, we can easily take the retardation effect into account and the cross section for electron ejection by the projectile is simply expressed by[15]

$$\frac{d^2\sigma^e}{dE_e\, d\Omega_e} = \frac{Z_T Z_p^2 e^4}{m_e V_p^2 E_e^2} \delta\left(\cos\theta_e - \frac{1}{V_p}\left(\frac{E_e}{2m_e}\right)^{1/2}\right), \tag{10}$$

where $E_e$ is the energy of ejected electron and $\theta_e$ is the ejection angle with respect to the incident beam. The cross section for bremsstrahlung produced by the interaction between the ejected electron and a target nucleus is given by Eq. (1) by replacing $T_r$, $Z_T$, and $Z_p$, respectively, with the ejected-electron energy 1 and the atomic number of target nucleus. Using Eqs. (1) and (9) and Ref. 7, the production cross section for the SEB is expressed by

$$\frac{d^2\sigma^{\mathrm{SEB}}}{d\Omega_L d(\hbar\omega_L)}(\theta_L,\hbar\omega_L)=\frac{2\alpha r_0^2}{\pi}Z_p^2 Z_T^2\frac{1}{\hbar\omega_L}\frac{m_e C^2}{T_m}\int_1^{T_r/\hbar\omega}\frac{dt}{t^2}\int_1^t ds f(s,t,\theta_L)\frac{1}{\ln(1.16s\hbar\omega/\bar{I})}, \tag{11}$$

where

$$f(s,t,\theta_L)=C_1+C_2\sin^2\theta_L+(B_1+B_2\sin^2\theta_L)\cos\theta_L,$$

with

$$C_1=\left(g_0+g_1 t\frac{\hbar\omega}{T_m}\right)g(\xi_0,\xi),$$

$$C_2=\tfrac{1}{2}g_1\left(1-3t\frac{\hbar\omega}{T_m}\right)g(\xi_0,\xi),$$

$$B_1=\frac{\beta_0}{2}\left(t\frac{\hbar\omega}{T_m}\right)^{1/2}\left(g_2+g_3 t\frac{\hbar\omega}{T_m}\right)g(\xi_0,\xi),$$

$$B_2=\frac{\beta_0}{2}\left(t\frac{\hbar\omega}{T_m}\right)^{1/2}g_3\left(\tfrac{3}{2}-\tfrac{5}{2}t\frac{\hbar\omega}{T_m}\right)g(\xi_0,\xi),$$

$$g_0=(3-T)\tfrac{1}{4}\ln\left(\frac{1+\sqrt{T}}{1-\sqrt{T}}\right)+\frac{\sqrt{T}}{2},$$

$$g_1=(3T-1)\tfrac{1}{4}\ln\left(\frac{1+\sqrt{T}}{1-\sqrt{T}}\right)-\tfrac{3}{2}\sqrt{T},$$

$$g_2=(\tfrac{19}{4}-\tfrac{17}{2}T+\tfrac{9}{4}T^2)\ln\left(\frac{1+\sqrt{T}}{1-\sqrt{T}}\right)+8\sqrt{T},$$

$$g_3=(\tfrac{27}{2}T-\tfrac{13}{4}-\tfrac{15}{4}T^2)\ln\left(\frac{1+\sqrt{T}}{1-\sqrt{T}}\right)-12\sqrt{T},$$

$$T=1-\frac{1}{s},\quad \beta_0=\left(2s\frac{\hbar\omega}{m_e C^2}\right)^{1/2},$$

$$T_m=4\frac{m_e}{m_p}E_p,\quad g(\xi_0,\xi)=\frac{\xi(1-e^{-2\pi\xi_0})}{\xi_0(1-e^{-2\pi\xi})},$$

$$\xi_0=Z_T\left(\frac{\mathcal{R}}{\hbar\omega s}\right)^{1/2}\text{ and }\xi=\xi_0/\sqrt{T}.$$

Since $E_p$ is the projectile energy, $T_m$ is the maximum energy that can be transferred from the projectile to a free electron; $t$ and $s$ represent, respectively, the initial energy of the ejected electron and its energy passing in the target material, and $\bar{I}$ is the mean ionization potential.[16]

## IV. COMPARISON WITH EXPERIMENT

In the continuum spectra shown in Fig. 1, we can obviously distinguish two components of the continuum x rays; the one is QFEB and the other one which extends to the high-energy region is considered to be mainly SEB. Since it has been confirmed that $\hbar\omega_L d^2\sigma^{\mathrm{SEB}}(\theta_L,\hbar\omega_L)/d\Omega_L d(\hbar\omega_L)$ is a monotonic function of $\hbar\omega_L$,[5,7] SEB is approximately expressed by

$$\hbar\omega_L\frac{d^2\sigma^{\mathrm{SEB}}}{d\Omega_L d(\hbar\omega_L)}(\theta_L,\hbar\omega_L)=\sum_{n=0}a_n(\theta_L)(\ln\hbar\omega)^n. \tag{12}$$

The coefficients $a_n$ can be determined from least-squares fit to the experimental spectral region where QFEB does not contribute. Here, the order $n$ in Eq. (12) is taken as $n\leq 2$; this gives the most reasonable fit. The curves $\hbar\omega_L d^2\sigma^{\mathrm{SEB}}(\theta_L,\hbar\omega_L)/d\Omega_L d(\hbar\omega_L)$ thus determined are shown in Fig. 1 as the background for QFEB. As the result of this estimation of the background, we are able to discuss quantitatively QFEB. In the low-energy part of the spectra, we can see two small peaks of characteristic $K$ x rays from Fe and Ni impurities. These peaks become clearly distinguishable in the backward directions, since the intensity of the continuum x rays decreases in backward directions while the characteristic x rays are isotropic. Nevertheless, the peaks are not so large as to affect the general feature of the continuum x rays, which is now under consideration.

In Fig. 1, the curves that agree well with the experimental QFEB are the sum of the SEB calculated from Eq. (12) and QFEB calculated from Eq. (5). It can be seen in this figure that the agreement between the theory and the experiment is quite satisfactory except in the region near the end point of QFEB. In particular, the angular

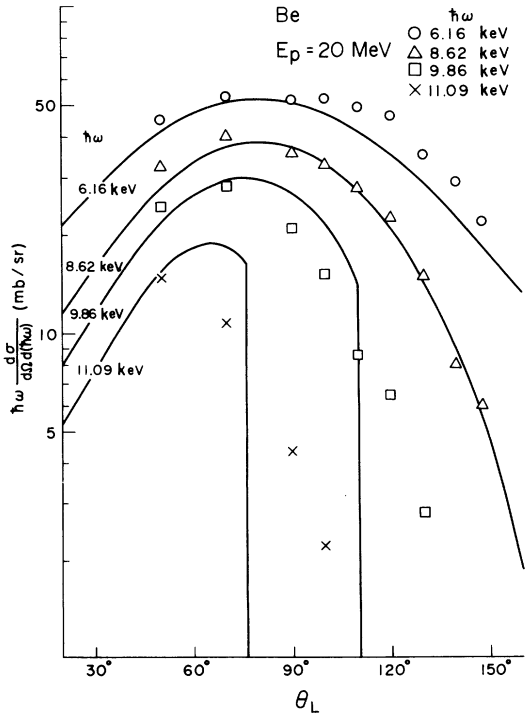


FIG. 2. Angular distributions of QFEB. The solid curves are theoretical predictions obtained from Eq. (5).

dependence of the QFEB spectrum originating from the Doppler effect—$\hbar\omega_{end} = T_\gamma(1-\beta^2)^{1/2}/(1-\beta\cos\theta_L)$—is well reproduced by the theory. Angular distributions of QFEB obtained by subtracting the SEB are shown in Fig. 2, together with those calculated from Eq. (5). Here again the agreement between the experiment and the theory is quite good except in the region near the end-point energy. The production cross section for QFEB given by Eq. (5) is discontinuous at the end-point energy $\hbar\omega_{end}$ because of the correction for Coulomb deflection—$g(\xi_0, \xi)$. As seen in Fig. 1, however, the experimental spectra of QFEB near the end-point energy continue to a region higher than $\hbar\omega_{end}$ and gradually decrease to zero. In order to interpret this behavior, first the energy spread of incident beam is to be considered. Proton beams of 20 MeV bombarded the Be target of 46 mg/cm$^2$, so that the effective energy spread in the target is estimated to be $19.22 \pm 0.78$ MeV at $\theta_L = 90°$. This energy spread of the proton beam results in the spectral spread of only $\pm 0.42$ keV at the end-point energy of QFEB. Next, the spectrum of QFEB obtained at $\theta_L = 90°$ is compared with theoretical calculations in Fig. 3, where the dot and dashed curve is calculated from Eq. (5) and the solid curve is obtained from Eq. (8) taking account of the velocity distributions of Be 1$s$ and 2$s$ electrons. It is found in this figure that Eq. (8) is in excellent agreement with the experiment and the velocity distribution of orbital electrons has considerable effect on the spectral shape near the end point. As in the case of radiative electron capture,[17] QFEB is therefore a process which reflects the velocity distribution of the orbital electrons and is expected to be useful in obtaining information on orbital electrons.

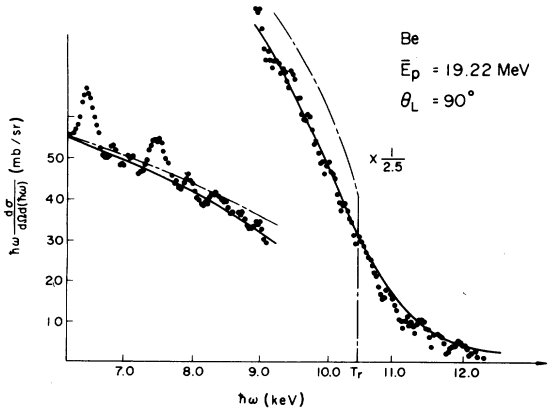


FIG. 3. The QFEB spectrum near the end-point energy obtained at $\theta_L = 90°$ subtracting the SEB calculated from Eq. (12). The dot and dashed curve shows the prediction from Eq. (5) and the solid curve was calculated from Eq. (8) by taking account of the velocity distribution of orbital electrons.

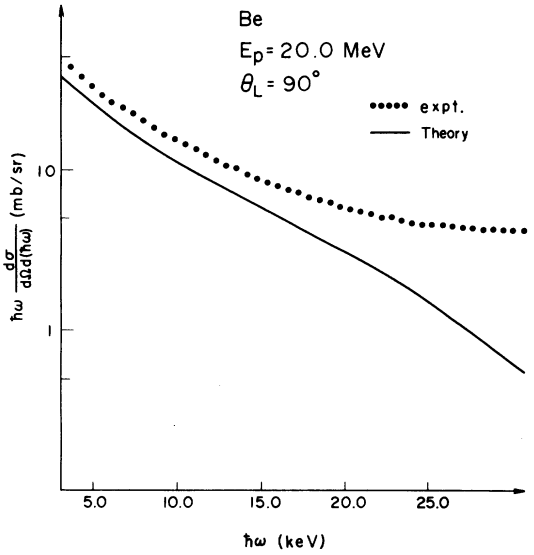


FIG. 4. The energy spectrum of SEB obtained at $\theta_L = 90°$. The dotted curve shows the least-squares fit of Eq. (12) to the experimental result, and the solid line is the theoretical one calculated from Eq. (11).

In Fig. 4, the energy spectrum of SEB obtained at $\theta_L = 90°$ is compared with that calculated from Eqs. (11) and (12). In the low-energy region, the spectral shape agrees well, whereas the calculated cross sections underestimate the experimental cross sections by about 25%. In the high-energy region, however, disagreement between the theory and the experiment is large. Angular distributions of SEB are shown in Fig. 5, together with those calculated from Eq. (11). Here again,

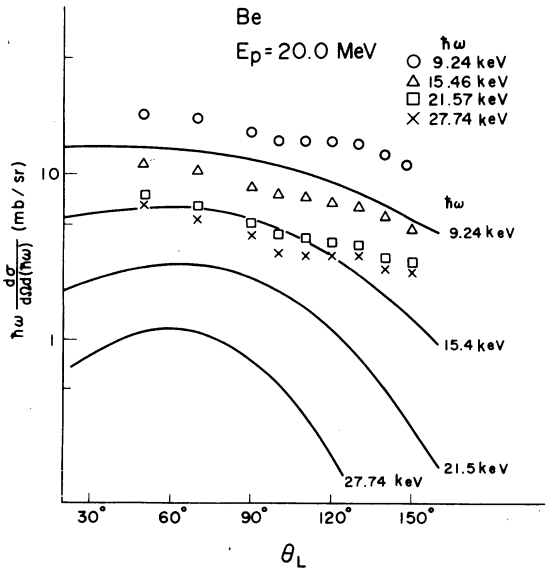


FIG. 5. Angular distributions of SEB. The solid curves were calculated from Eq. (11).

agreement between the theoretical and experimental angular dependence seems to be rather good in the low-energy region, while in the high-energy region, the theory predicts the angular dependence stronger than the experiment. Besides SEB, there may be contributions to the measured continuum x rays from the nuclear bremsstrahlung produced by the interaction between the projectile and the target nucleus. It was, however, confirmed by a calculation using a dipole approximation[18] that this contribution is quite negligible. Furthermore, the background attributed to Compton-scattered $\gamma$ rays from nuclear reactions is expected to show a flat spectrum in contrast to the present one as was previously[10] reported.

## V. SUMMARY

Continuum x rays produced by the bombardment of the Be target with 20-MeV protons were measured over the angular range $\theta_L = 50-148°$. The Doppler effect of QFEB was clearly observed depending on the observation angle. Theories of QFEB and SEB were developed under the assumption that the orbital electron is free and at rest. The results of calculation of QFEB can quite well reproduce the experiment. In particular, the spectral shape of QFEB near the end-point energy markedly reflects the velocity distribution of orbital electrons. This result suggests that QFEB would provide a useful method for studying the state of valence electrons. The present calculation of SEB taking into account the retardation effect gives rather good agreement with the experimental result in the low-x-ray-energy region, but not in the high-energy region.

[1]H. W. Schnopper, J. P. Delvaille, K. Kalata, A. R. Sohval, M. Abdulwahab, K. W. Jones, and H. E. Wegner, Phys. Lett. 47A, 61 (1974).
[2]A. R. Sohval, J. P. Delvaille, K. Kalata, and H. W. Schnopper, J. Phys. B 8, L426 (1975).
[3]D. H. Jakubassa and M. Kleber, Z. Phys. A 273, 29 (1975).
[4]A. R. Sohval, J. P. Delvaille, K. Kalata, K. Kirby-Docken, and H. W. Schnopper, J. Phys. B 9, L25 (1976).
[5]F. Folkmann, C. Gaarde, T. Huus, and K. Kemp, Nucl. Instrum. Methods 116, 487 (1974).
[6]F. Folkmann, J. Borggreen, and A. Kjeldgaard, Nucl. Instrum. Methods 119, 117 (1974).
[7]K. Ishii, S. Morita, and H. Tawara, Phys. Rev. A 13, 131 (1976).
[8]K. Ishii, M. Kamiya, K. Sera, S. Morita, and H. Tawara, Phys. Rev. A 15, 2126 (1977).
[9]R. Anholt and T. K. Saylor, Phys. Lett. 56A, 455 (1976).
[10]A. Yamadera, K. Ishii, K. Sera, M. Sebata, and S. Morita, Phys. Rev. A (in press).
[11]K. Sera, K. Ishii, M. Kamiya, A. Kuwako, and S. Morita, Phys. Rev. A 21, 1412 (1980).
[12]Heitler, *The Quantum Theory of Radiation* (Clarendon, Oxford, England, 1954), p. 242.
[13]J. D. Jackson, *Classical Electrodynamics*, 2nd ed. (Wiley, New York, 1975), p. 522.
[14]H. Bethe and E. E. Salpeter, *Quantum Mechanics of One- and Two-Electron Atoms* (Plenum, New York, 1977), p. 39.
[15]T. F. M. Bonsen and L. Vriens, Physica (Utrecht) 47, 307 (1970).
[16]L. C. Y. Yuan and C. S. Wu, *Methods of Experimental Physics* (Academic, New York, 1961), Vol. 5A, p. 10.
[17]A. R. Sohval, J. P. Delvaille, K. Kalata, and H. W. Schnopper, J. Phys. B 9, L47 (1976).
[18]K. Alder, A. Bohr, T. Huus, B. Mottelson, and A. Winther, Rev. Mod. Phys. 28, 432 (1956).